Kinetics of Energy Selective Cs Encapsulation in Single-Walled Carbon Nanotubes for Damage-Free and Position-Selective Doping

Toshiaki Kato,*,[†] Erik C. Neyts,[‡] Yoshihiro Abiko,[†] Toshiki Akama,[†] Rikizo Hatakeyama,[†] and Toshiro Kaneko[†]

[†]Department of Electronic Engineering, Tohoku University, Sendai 980-8579, Japan
[‡]Research Group PLASMANT, Department of Chemistry, University of Antwerp, Universiteitsplein 1, 2610 Antwerp, Belgium

ⓢ Supporting Information

ABSTRACT: A method has been developed for damage-free cesium (Cs) encapsulation within single-walled carbon nanotubes (SWNTs) with fine position selectivity. Precise energy tuning of Cs-ion irradiation revealed that there is a clear energy window (20−60 eV) for the efficient encapsulation of Cs through the hexagonal network of SWNT sidewalls without causing significant damage. This minimum energy threshold of Cs-ion encapsulation (~20 eV) matches well with the value obtained by *ab initio* simulation (~22 eV). Furthermore, position-selective Cs encapsulation was carried out, resulting in the successful formation of pn-junction SWNT thin films with excellent environmental stability.
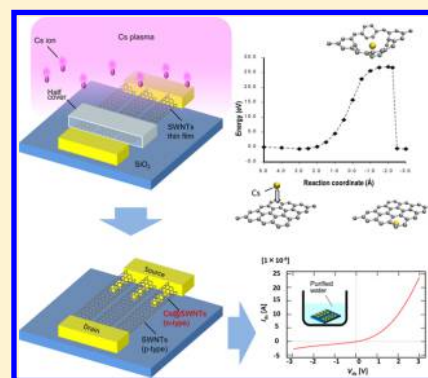
In the past decade, flexible electronics, namely mechanically flexible thin-film electrical devices, have been intensively investigated as an application of optoelectrical science.[1−3] Because of their outstanding fundamental features such as excellent carrier mobility, mechanical flexibility, and thermal conductance, single-walled carbon nanotubes (SWNTs) are one of the most promising candidate materials for next-generation high-performance flexible electronics such as thin-film transistors (TFTs),[4−6] light-emitting diodes,[7,8] and thermoelectric devices.[9,10] Fabrication of these devices requires precise control of the transport-type of SWNTs (between p- and n-type). Untreated pristine SWNT film shows p-type features due to hole doping by oxygen or water molecules,[11] whereas alternative electron doping is necessary to obtain n-type SWNTs (i.e., chemical doping).[12−14] Fabrication of n-type SWNT films has been reported using various chemical dopants, such as potassium (K),[12] polyethylenimine (PEI),[13] and tetracyano-p-quinodimethane (TCNQ).[14] However, most of those dopings were performed by exterior functionalization of SWNTs, where environmental resistance is very low. Fabrication of n-type SWNTs, which are stable in various environments such as air, water, and high-temperature conditions, is a critical issue for the practical use of SWNT thin films in future high-performance flexible electronics.

Encapsulation of foreign atoms and molecules within SWNTs is an alternative approach to chemical doping in SWNTs.[15,16] Since the dopants are enclosed by the carbon shell of the SWNTs, the stability of these materials is very high. Vacuum-vapor transfer is a well-known method for injecting foreign atoms and molecules into the open end of SWNTs. Since this method is easy and cost-effective, it is very useful to obtain the atoms and molecules encapsulated within SWNTs as bulk materials. However, the materials can be encapsulated only from the open end of SWNTs under relatively high temperatures (>500 °C). The high temperature process allows the encapsulated material to diffuse throughout the SWNT interior. Thus, it is difficult to demonstrate position-selective, local encapsulation in SWNTs by this method, which is important for producing complicated logic circuits such as pn-junction diodes,[17] inverters,[18] and ring oscillators[19] with p- and n-type SWNTs. Plasma-ion irradiation is another powerful tool for encapsulating atoms and molecules within SWNTs. Our group has encapsulated materials such as Cs, K, Na, Li, C_{60}, Ca, and I with this method.[20−25] Since energetic ions pass through the hexagonal carbon network of SWNT sidewalls at room temperature, selective encapsulation of foreign atoms and molecules can be performed with high position selectivity. However, the energetic ions sometimes break the SWNT's carbon bonds, resulting in degraded device performance. Therefore, the development of a damage-free, position-selective encapsulation process is important for creating high-performance SWNT thin-film devices with high environmental stability.

Here, we demonstrate the successful damage-free and position-selective encapsulation of Cs into SWNTs. The minimum energy threshold (~20 eV) for the encapsulation of Cs into SWNTs was revealed through the precise tuning of Cs irradiation energy (E_i). Computational studies were also
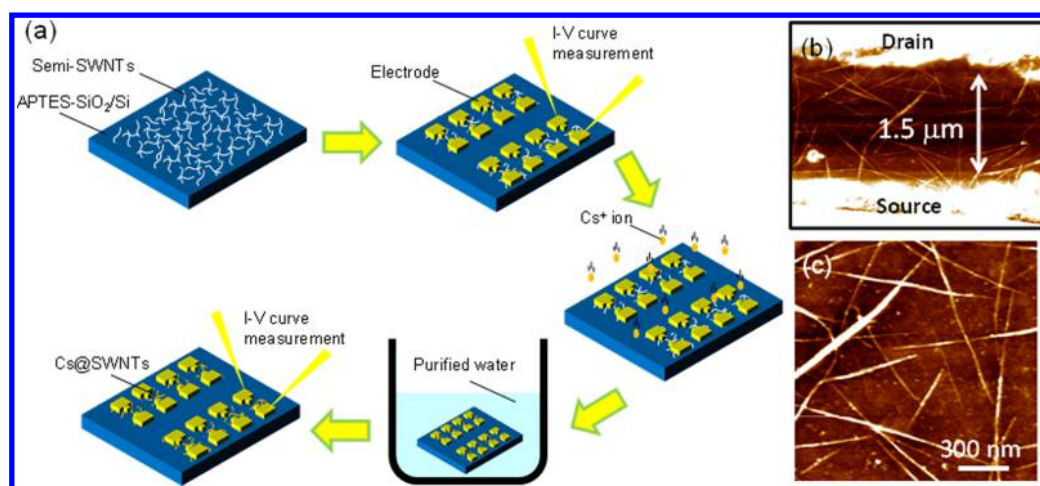
Figure 1. (a) Schematic illustration of experimental progression for Cs-ion irradiation to SWNT-TFTs. Au electrodes were fabricated on the SWNT networks by photolithography. Then, Cs-ion irradiation was carried out on the SWNT-TFTs. After the careful rinsing of Cs from the exterior of the SWNTs (using purified water), electrical measurements of Cs irradiated SWNT-TFTs were carried out by a vacuum probe station. (b, c) Typical (b) low- and (c) high-magnification atomic force microscopy images of SWNT-TFTs.
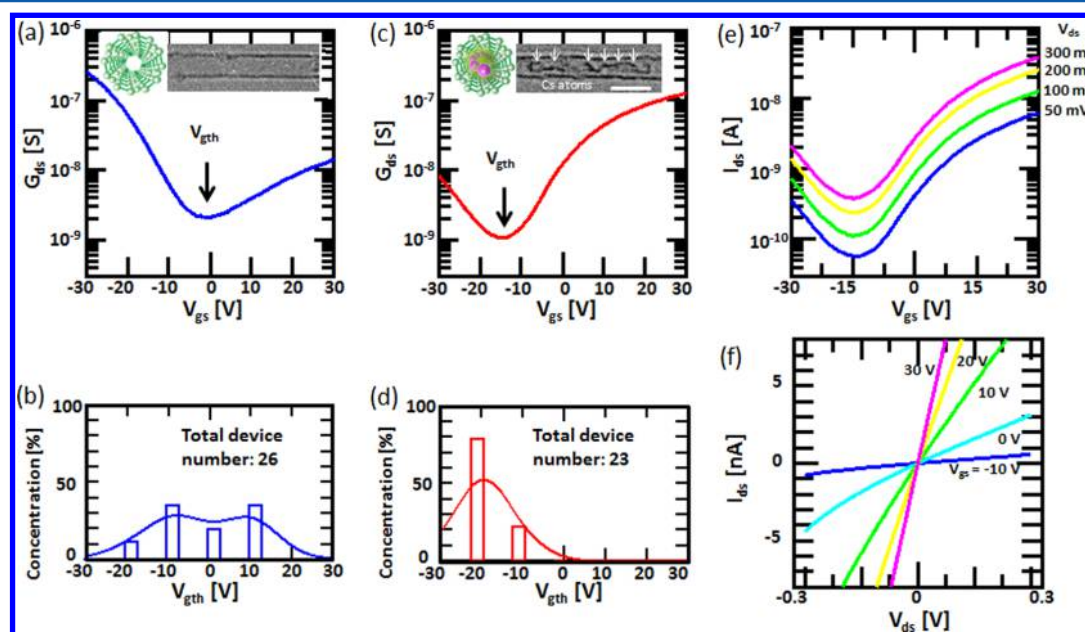

Figure 2. (a–d) Typical (a, c) I_{ds}–V_{gs} curves and (b, d) histograms of V_{gth} (a, b) before and (c, d) after Cs-ion irradiation. (e, f) (e) I_{ds}–V_{gs} and (f) I_{ds}–V_{ds} curves of Cs irradiated SWNT-TFTs, measured at various V_{ds}, and V_{gs} values, respectively. The insets of (a) and (c) show typical transmission electron microscope image of pristine SWNTs and Cs@SWNTs, respectively. The scale bar in the inset of (c) is 2 nm.

carried out to elucidate the kinetics of the Cs ions' incorporation into SWNTs, obtaining a consistent threshold energy (~22 eV) for Cs encapsulation. Furthermore, position-selective Cs encapsulation was realized by the combination of damage-free Cs encapsulation and a polymer capping method, resulting in the successful fabrication of pn-junction SWNTs with high environmental stability.

Figure 1a shows a schematic of the basic experimental process. First, SWNT-TFTs were fabricated by a conventional photolithography technique. Then, Cs ions were irradiated via plasma-ion irradiation with fine energy tuning. The electrical features of the Cs-irradiated SWNT-TFTs were measured in a vacuum-probe station, followed by a careful rinse of Cs atoms from the exterior of the SWNTs using purified water. Further detailed experimental conditions are listed in the Methods section and the Supporting Information.

Energy-controlled irradiation of Cs was realized by plasma-ion irradiation.[20−25] The energy of Cs ions entering the SWNTs was estimated by the energy difference between the plasma potential and substrate bias, which was controlled by varied dc bias voltages applied to the substrate (see Supporting Information). In order to avoid uncertain effects such as Cs depth-wise penetration into the SWNT film, very thin SWNT networks were used (Figure 1b,c).

First, Cs irradiation with constant irradiation energy (60 eV) was carried out on the SWNT-TFTs. The source−drain current (I_{ds}) versus gate bias (V_{gs}) voltage curves show that the p-type current (I_{onp}) is higher than the n-type current (I_{onn}) prior to Cs irradiation (Figure 2a). The threshold voltage of the gate bias (V_{gth}) is distributed mostly for V_{gs} ranging between −20 and 20 V (Figure 2b), whereas I_{onn} becomes higher than I_{onp} (Figure 2c) and the histogram of V_{gth} drastically shifts toward

the negative V_{gs} direction (Figure 2d) after Cs irradiation. This indicates that the Cs atoms have been encapsulated, acting as electron donors to the SWNTs, which results in the transition of carrier type from p-type to n-type for the SWNT-TFTs (Figure 2c−f). Note that the entire device was carefully rinsed by purified water (over 8 h). Thus, the effect of Cs atoms on the exterior of the SWNTs may be negligible (see Supporting Information). This also indicates that the encapsulated Cs atoms are stable in water.

In addition to examining the stability of Cs-encapsulated SWNTs (Cs@SWNTs) in water, high-temperature stability was investigated. It should be noted that the n-type features were stable even after high-temperature annealing at 400 °C (see Supporting Information); this is very important for the practical application of SWNT-based flexible electronics.

In order to identify the threshold energy for Cs-ion encapsulation, similar experiments were carried out under various ion-energy conditions. Here, we use the ratio of I_{onn} to I_{onp} as an indicator of transport type of SWNT-TFTs; i.e., $I_{onn} < I_{onp}$ and $I_{onn} > I_{onp}$ denote p-type and n-type dominant conduction, respectively. Interestingly, a clear ion-energy dependence on transport type can be produced, as shown in Figure 3a. I_{onn} was lower than I_{onp} for the low-energy range (≤5
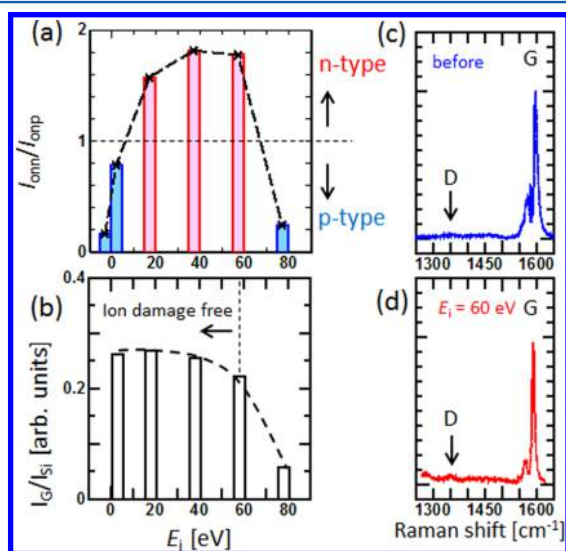

Figure 3. (a, b) Plots of (a) I_{onn}/I_{onp} and (b) I_G/I_{si} as a function of E_i. (c, d) Typical raw Raman scattering spectra of (c) before and (d) after Cs irradiation (E_i = 60 eV).

eV), indicating that Cs ions cannot be encapsulated at such energies. Meanwhile, I_{onn} becomes higher than I_{onp} in the range $20 \leq E_i \leq 60$ eV. Then, I_{onn} had lower values than I_{onp} for higher energies (≥80 eV). This indicates that Cs ions were encapsulated for a specific energy window ($20 \leq E_i \leq 60$ eV).

Further detailed kinetics of Cs-ion encapsulation into SWNTs was investigated by systematic density-functional theory (DFT) simulations. Details of the simulation method are provided in the Methods section. The SWNT is represented by a flat, periodic, fully relaxed 4×4 unit-cell graphene sheet containing 32 atoms. Initially, the Cs atom is positioned 5 Å above the graphene sheet. All carbon atoms are then allowed to relax, using the conjugate-gradient algorithm, until no forces exceed 0.01 eV/Å. However, in order to maintain the designated distance of 5 Å between the Cs atom and the graphene sheet, six carbon atoms at the edge of the graphene

sheet are kept fixed in the z-direction, effectively preventing the graphene sheet from rotating or translating in the z-direction. No constraints are applied in the lateral directions, thus allowing the sheet to expand (or contract) upon interaction with the Cs atom. After minimization, the resulting output structure of the graphene sheet is used as input for the next simulation, in which the Cs atom is now positioned 4 Å above the sheet. The Cs−graphene distances calculated in this way are {5.0, 4.0, 3.0, 2.5, 2.0, 1.5, 1.0, 0.5, 0.0, −0.5, −1.0, −1.5, −2.0, −2.5, −3.0} Å. Since these distances are sampled consecutively, with each iteration using the final structure from the previous step as its input, this procedure allows for a mapping of the energy barrier along the selected reaction coordinate. While employing a flat surface to represent a curved nanotube will certainly affect the Cs adsorption energies, the reaction barrier for penetration is expected to be fairly insensitive to the curvature effect.

Specifically, three reaction coordinates are studied. These reaction coordinates consist of straight vertical paths, which translate the Cs atom from above the graphene sheet, pass through the sheet, to an end point below it. The initial positions of the Cs are above a hexagon ("rc-hex"), above a bond ("rc-bond"), or above an atom ("rc-atom"). Note that curved paths are considered irrelevant, given the high impact energy of the Cs ions in the experiment.

In Figures 4a through 4c, reaction paths for the three reaction coordinates are shown. In all three cases, the Cs ion is found to bind weakly to the graphene sheet at a distance of 3.0 Å, with binding energies of 0.61 eV, 0.57 and 0.57 eV for rc-hex, rc-bond, and rc-atom, respectively. In the rc-hex case, the transition state is observed at a distance of −2.0 Å from the (original) plane of the graphene sheet. The corresponding barrier energy is calculated to be 27.51 eV. In the transition state, the carbon atoms are pushed out-of-plane downward as well as laterally, thus creating a hole in the graphene sheet, allowing the Cs atom to enter. After the Cs passes through the graphene sheet, the hole quickly jumps back, thereby restoring the original defect-free graphene-sheet structure. In the rc-bond case, the transition state occurs at a distance of −1.0 Å. The energy barrier is found to be 22.70 eV. Again, a hole in the graphene layer is created, although in this case, only three C−C bonds are broken, whereas four C−C bonds are broken in the rc-hex case. Again, after the Cs passes through the graphene sheet, the original structure is restored. Finally, in the rc-atom case, the transition state is found at a distance of −0.5 Å, and the corresponding energy barrier is calculated to be 22.14 eV. In this case, the original structure is not restored after the Cs passed the graphene sheet. Instead, a hole is created, with a single carbon atom bonded only to one other carbon. In our static approximation, this hole is permanent, as shown in Figure 4c. It is likely, however, that thermal fluctuations will cause the carbon network to revert to its original structure. This has, for instance, been observed in both classical and *ab initio* molecular dynamics simulations of Ni implantation in buckyballs, forming endohedral Ni-metallofullerenes.[26,27]

The threshold value for Cs-ion encapsulation (22.14−27.51 eV) obtained from the computer simulations matches well with that of the experimental results (~20 eV) (Figure 3a). Furthermore, the simulation results provide evidence that bond healing may occur after Cs encapsulation by thermal fluctuations, indicating that damage-free encapsulation may possible with energy-controlled Cs-ion irradiation.
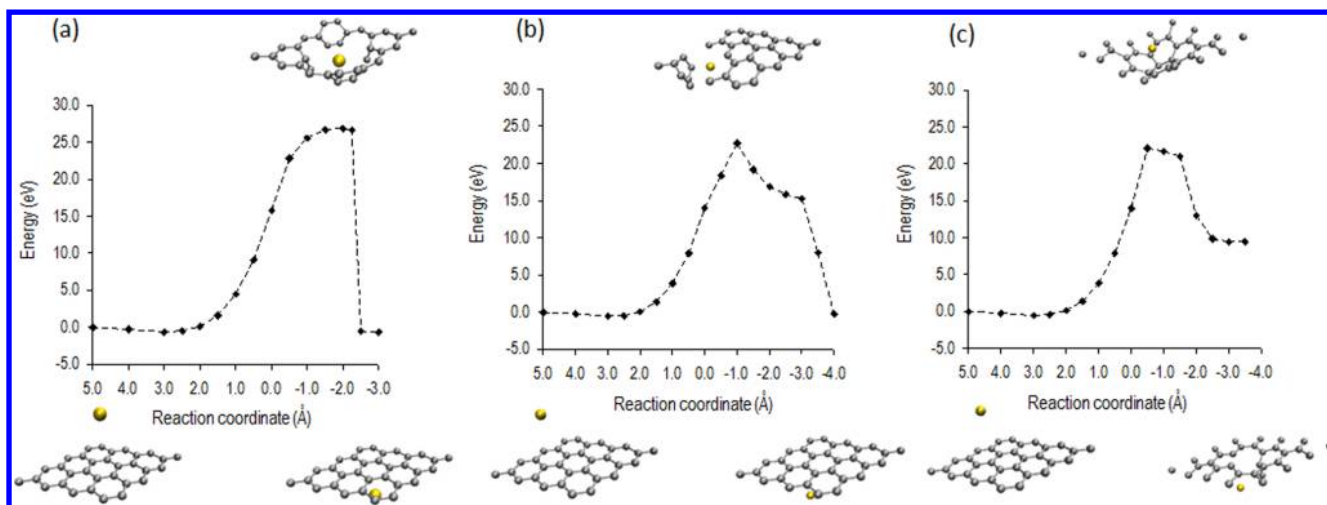
Figure 4. (a−c) Calculated energy evolution along the reaction coordinate, starting with the Cs atom located (a) above the central hexagon of the graphene sheet at rc = 5 Å, (b) above a C−C bond in the graphene sheet at rc = 5 Å, and (c) above a C atom in the graphene sheet at rc = 5 Å. The values on the x-axis denote the distance between the Cs atom and the z-constrained carbon atoms. The reported energies are relative to the initial structure at 5 Å. After impact, the original graphene sheet structure is restored.
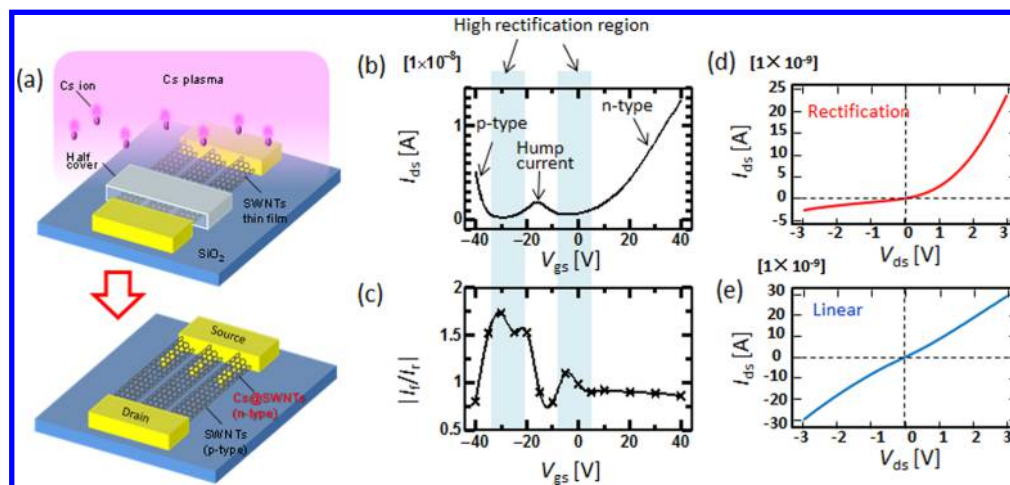

Figure 5. (a−c) (a) Schematic illustration, (b) typical I_{ds}−V_{gs} curves, and (c) I_f/I_r as a function of V_{gs} for the position-selective Cs-ion irradiation of SWNT-TFTs. (d, e) I_{ds}−V_{ds} behavior for different V_{gs} conditions [(d) V_{gs} = −30 V and (e) V_{gs} = 10 V].

To verify the accuracy of our simulation results in terms of damage, Raman scattering measurements were carried out for the Cs-ion-irradiated SWNTs under various energy conditions. We use the G-band intensity (I_G) normalized by the intensity of silicon substrate (I_{si}) (I_G/I_{Si}) as an indicator of SWNT quality on the substrate (instead of the G/D ratio) because high-energy ion bombardment easily removes SWNTs from the substrate and the reduction of G-band intensity was dramatic compared with the changes in the D-band. It is found that I_G/I_{Si} is nearly constant for ion energies up to 60 eV, whereas drastic reduction is observed above 80 eV (Figure 3b). This indicates that significant damage can be caused at ion energies above 80 eV, which is consistent with the I_{onn}/I_{onp} plot as a function of ion energy (Figure 3a). The damage free Cs encapsulation can also be confirmed through the comparison of the raw Raman scattering spectra before (Figure 3c) and after (Figure 3d) Cs irradiation (E_i = 60 eV). The G-band to D-band ratio does not show significant change even after the Cs irradiation, indicating the inducing of damage during Cs irradiation can be negligible in this energy range (E_i < 60 eV). The transition from n-type to p-type conduction is observed with E_i increasing from 60 to 80

eV. This shows that Cs ions cannot be stabilized in SWNTs under high-energy conditions (80 eV) because of their high kinetic energy. This result also indicates that significant damage does not occur within the optimal energy window (20 ≤ E_i ≤ 60 eV) for Cs-ion encapsulation.

Since damage-free Cs encapsulation becomes possible by energy-controlled Cs-ion irradiation, we attempted to perform damage-free Cs encapsulation at localized areas in SWNT-TFTs. In consideration of local doping, we focused on the pn-junction diode,[17] which is one of the most important basic components for logic circuits. The fabrication of pn-junction SWNTs was carried out in combination with damage-free Cs encapsulation and half-covered polymer capping via photo-lithography (Figure 5a). The results of electrical measurements show that polymer capping can effectively block Cs ions (see Supporting Information), indicating that local encapsulation of Cs may be possible. A typical I_{ds}−V_{gs} curve is shown for Cs-doped SWNT-TFTs with half cover polymer cap (Figure 5b). In addition to conventional p-type and n-type current, hump-current features were clearly observed between p- and n-type regions (Figure 5b). In order to identify the origin of this hump

current, systematic investigations were carried out for the pristine SWNT-TFTs with electrical doping by dual top gates, which can form an ideal pn junction by controlling the top-gate bias voltages.[28] In particular, hump-current features can also be observed in an ideal pn-junction device with electrical doping (see Supporting Information), meaning that the origin of the hump current can be attributed to pn-junction structures; i.e., a pn junction was successfully formed by the position-selective and damage-free Cs encapsulation within SWNT thin films. In fact, similar hump currents can be also observed for pn junctions of individual SWNTs, owing to the tunneling current between pn-junction regions.[17,22] The forward-to-reverse current ratio (I_f/I_r) in the I_{ds}–V_{ds} curve is plotted as a function of V_{gs} (Figure 5c). Interestingly, a high I_f/I_r occurs only near the tail region of the hump current (Figure 5d), and other V_{gs} conditions show a linear I_{ds}–V_{ds} behavior without any rectification features (Figure 5e). This can also be explained by the band-structure model of pn-junction SWNTs. Since the band structure for $V_{gs} \sim -40$ V and $V_{gs} > 20$ V can indicate p^+p and nn^+ junctions, respectively, current can travel both in the forward and reverse directions, resulting in the suppression of rectification features. Because the tunneling current can also go through the pn junction, rectification features are also suppressed in the hump-current region ($V_{gs} \sim -18$ V).[17] Thus, an ideal pn junction can only be formed with V_{gs} at around −30 and 0 V, where clear rectification features are observed.

The density of Cs atoms in SWNTs should also effect on the electrical transport properties of SWNTs as well as the irradiation energy of Cs ions discussed in this paper. Although it is very difficult to accurately identify the density of Cs, it can be conjectured that the density of Cs may have a correlation with the on/off ratio of SWNTs-TFT. If higher density of Cs can be encapsulated in SWNTs, the Fermi level of SWNTs can shift over the conduction band, resulting in the weak gate bias dependence of I_{ds}. At the current situation, such kind of semiconductor to metallic transition of SWNTs cannot be observed within our experimental conditions. This indicates the doping density of Cs in this study may be relatively low compared with that of carbon in SWNTs. The fabrication of metallic nanowire with densely Cs encapsulated semiconducting SWNTs can be the next target relating with this topics.

In conclusion, damage-free and position-selective Cs encapsulation has been realized by an energy-controlled Cs-ion-irradiation method. Based on our systematic investigations, a clear energy window of Cs-ion irradiation for the efficient encapsulation into SWNTs was determined ($20 \leq E_i \leq 60$ eV). Furthermore, the minimum threshold energy for Cs encapsulation matches well with the simulation results, indicating that Cs ions can be encapsulated through the hexagonal network of SWNT sidewalls—without destroying the network because of the self-healing process. A highly position-selective Cs encapsulation method was also developed, resulting in the successful formation of pn-junction SWNT films with clear rectification features. Since the Cs@SWNTs produced by this method exhibit high environmental stability [air, water, and high temperature (~400 °C)], this method is useful for the practical application of SWNT-based high-performance flexible electronics.

METHODS

Fabrication of SWNT-TFTs. High-purity semiconductor SWNTs (Nanointeglis, 99%) were used in this study. SWNTs with the diameter of 1.2−1.7 nm were coated on a SiO_2 (300 nm)/Si substrate. Prior to the SWNT coating, (3-aminopropyl)triethoxysilane (APTES) was coated on the surface of the SiO_2 to enhance the adsorption of SWNTs and produce dense networks of thin SWNTs. Pairs of Au electrodes were fabricated on top of the SWNTs using photolithography. The channel length of the SWNTs was 1.5 μm. SWNTs outside of the channel region were removed by oxygen plasma treatment.

Computer Simulation. The DFT calculations in the generalized gradient approximation (GGA) were performed using the Vienna *ab initio* Simulation Package (VASP).[29,30] Exchange and correlation were calculated according to the Perdew−Burke−Ernzerhof functional.[31] The energy cutoff for the plane-wave expansion was set to 400 eV. Projector-augmented wave (PAW) potentials were used to represent the ionic cores.[32] A $6 \times 6 \times 1$ Monkhorst−Pack k-point mesh was used to sample the Brillouin zone. A vacuum region of 15 Å was used in the z-direction.

ASSOCIATED CONTENT

Ⓢ Supporting Information

Experimental apparatus for Cs-ion irradiation; typical plasma characteristics measured by a Langmuir prove; stabilities of Cs@SWNTs in water and under high temperature conditions; effects of polymer caps on Cs-ion irradiation; pristine SWNT-TFTs with electrical doping by dual top gates. The Supporting Information is available free of charge on the ACS Publications website at DOI: 10.1021/acs.jpcc.5b00300.

AUTHOR INFORMATION

Corresponding Author

*E-mail kato12@ecei.tohoku.ac.jp; Ph +81-22-795-7046 (T.K.).

Notes

The authors declare no competing financial interest.

REFERENCES

(1) Ju, S.; Facchetti, A.; Xuan, Y.; Liu, J.; Ishikawa, F.; Ye, P.; Zhou, C.; Marks, T. J.; Janes, D. B. Fabrication of Fully Transparent Nanowire Transistors for Transparent and Flexible Electronics. *Nat. Nanotechnol.* **2007**, *2*, 378−384.

(2) Fan, Z.; Razavi, H.; Do, J.; Moriwaki, A.; Ergen, O.; Chueh, Y.-L.; Leu, P. W.; Ho, J. C.; Takahashi, T.; Reichertz, L. A.; et al. Three Dimensional Nanopillar Array Photovoltaics on Low Cost and Flexible Substrates. *Nat. Mater.* **2009**, *8*, 648−653.

(3) Kaltenbrunner, M.; White, M. S.; Głowacki, E. D.; Sekitani, T.; Someya, T.; Sariciftci, N. S.; Bauer, S. Ultrathin and Lightweight Organic Solar Cells with High Flexibility. *Nat. Commun.* **2012**, *3*, 1−7.

(4) Cao, Q.; Kim, H.-S.; Pimparkar, N.; Kulkarni, J. P.; Wang, C.; Shim, M.; Roy, K.; Alam, M. A.; Rogers, J. A. Medium-Scale Carbon Nanotube Thin-Film Integrated Circuits on Flexible Plastic Substrates. *Nature* **2008**, *454*, 495−500.

(5) Wang, C.; Zhang, J.; Ryu, K.; Badmaev, A.; Arco, L. G. D.; Zhou, C. Wafer-Scale Fabrication of Separated Carbon Nanotube Thin-Film Transistors for Display Applications. *Nano Lett.* **2009**, *9*, 4285−4291.

(6) Sun, D.-M.; Timmermans, M. Y.; Tian, Y.; Nasibulin, A. G.; Kauppinen, E. I.; Kishimoto, S.; Mizutani, T.; Ohno, Y. Flexible High-Performance Carbon Nanotube Integrated Circuits. *Nat. Nanotechnol.* **2011**, *6*, 156−161.

(7) Zhang, D.; Ryu, K.; Liu, X.; Polikarpov, E.; Ly, J.; Tompson, M. E.; Zhou, C. Transparent, Conductive, and Flexible Carbon Nanotube Films and Their Application in Organic Light-Emitting Diodes. *Nano Lett.* **2006**, *6*, 1880−1886.

(8) Mueller, T.; Kinoshita, M.; Steiner, M.; Perebeinos, V.; Bol, A. A.; Farmer, D. B.; Avouris, P. Efficient Narrow-Band Light Emission from a Single Carbon Nanotube P−N Diode. *Nat. Nanotechnol.* **2010**, *5*, 27−31.

(9) Small, J. P.; Perez, K. M.; Kim, P. Modulation of Thermoelectric Power of Individual Carbon Nanotubes. *Phys. Rev. Lett.* **2003**, *91*, 256801−1−4.

(10) Nonoguchi, Y.; Ohashi, K.; Kanazawa, R.; Ashiba, K.; Hata, K.; Nakagawa, T.; Adachi, C.; Tanase, T.; Kawai, T. Systematic Conversion of Single Walled Carbon Nanotubes into N-Type Thermoelectric Materials by Molecular Dopants. *Sci. Rep.* **2013**, *3*, 1−7.

(11) Derycke, V.; Martel, R.; Appenzeller, J.; Avouris, P. Controlling Doping and Carrier Injection in Carbon Nanotube Transistors. *Appl. Phys. Lett.* **2002**, *80*, 2773−2775.

(12) Javey, A.; Tu, R.; Farmer, D. B.; Guo, J.; Gordon, R. G.; Dai, H. High Performance N-type Carbon Nanotube Field-Effect Transistors with Chemically Doped Contacts. *Nano Lett.* **2005**, *5*, 345−348.

(13) Shim, M.; Javey, A.; Kam, N. W. S.; Dai, H. Polymer Functionalization for Air-Stable n-Type Carbon Nanotube Field-Effect Transistors. *J. Am. Chem. Soc.* **2001**, *123*, 11512−11513.

(14) Takenobu, T.; Takano, T.; Shiraishi, M.; Murakami, Y.; Ata, M.; Kataura, H.; Achiba, Y.; Iwasa, Y. Stable and Controlled Amphoteric Doping by Encapsulation of Organic Molecules Inside Carbon Nanotubes. *Nat. Mater.* **2003**, *2*, 683−688.

(15) Smith, B. W.; Monthioux, M.; Luzzi, D. E. Encapsulated C_{60} in Carbon Nanotubes. *Nature* **1998**, *396*, 323−324.

(16) Okazaki, T.; Iizumi, Y.; Okubo, S.; Kataura, H.; Liu, Z.; Suenaga, K.; Tahara, Y.; Yudasaka, M.; Okada, S.; Iijima, S. Coaxially Stacked Coronene Columns inside Single-Walled Carbon Nanotubes. *Ang. Chem., Int. Ed.* **2011**, *50*, 4853−4857.

(17) Zhou, C.; Kong, J.; Yenilmez, E.; Dai, H. Modulated Chemical Doping of Individual Carbon Nanotubes. *Science* **2000**, *290*, 1552−1555.

(18) Liu, X.; Lee, C.; Zhou, C.; Han, J. Carbon Nanotube Field-Effect Inverters. *Appl. Phys. Lett.* **2001**, *79*, 3329−3331.

(19) Javey, A.; Wang, Q.; Ural, A.; Li, Y.; Dai, H. Carbon Nanotube Transistor Arrays for Multistage Complementary Logic and Ring Oscillators. *Nano Lett.* **2002**, *2*, 929−932.

(20) Jeong, G.-H.; Hatakeyama, R.; Hirata, T.; Tohji, K.; Motomiya, K.; Yaguchi, T.; Kawazoe, Y. Formation and Structural Observation of Cesium Encapsulated Single-Walled Carbon Nanotubes. *Chem. Commun.* **2002**, 152−153.

(21) Izumida, T.; Hatakeyama, R.; Neo, Y.; Mimura, H.; Omote, K.; Kasama, Y. Electronic Transport Properties of Cs-Encapsulated Single-Walled Carbon Nanotubes Created by Plasma Ion Irradiation. *Appl. Phys. Lett.* **2006**, *89*, 093121−1−3.

(22) Kato, T.; Hatakeyama, R.; Shishido, J.; Oohara, W.; Tohji, K. P-N Junction with Donor and Acceptor Encapsulated Single-Walled Carbon Nanotubes. *Appl. Phys. Lett.* **2009**, *95*, 083109−1−3.

(23) Jeong, G.-H.; Hirata, T.; Hatakeyama, R.; Tohji, K.; Motomiya, K. C_{60} Encapsulation Inside Single-Walled Carbon Nanotubes using Alkali-Fullerene Plasma Method. *Carbon* **2002**, *40*, 2247−2253.

(24) Shishido, J.; Kato, T.; Oohara, W.; Hatakeyama, R.; Tohji, K. Modification of Electrical Transport Properties of Single-Walled Carbon Nanotubes Realized by Negative-Ion Irradiation with Electron-Free Pure Alkali-Halogen Plasma. *Jpn. J. Appl. Phys.* **2008**, *47*, 2044−2047.

(25) Shimizu, T.; Kato, T.; Oohara, W.; Hatakeyama, R. Electrical Transport Properties of Calcium Encapsulated Single-Walled Carbon Nanotubes Realized Using Calcium Plasma. *Jpn. J. Appl. Phys.* **2010**, *49*, 02BD05−1−3.

(26) Neyts, E. C.; Bogaerts, A. Formation of Endohedral Ni@C_{60} and Exohedral Ni−C_{60} Metallofullerene Complexes by Simulated Ion Implantation. *Carbon* **2009**, *47*, 1028−1033.

(27) Neyts, E. C.; Maeyens, A.; Pourtois, G.; Bogaerts, A. A Density-Functional Theory Simulation of the Formation of Ni-Doped Fullerenes by Ion Implantation. *Carbon* **2011**, *49*, 1013−1017.

(28) Lee, J. U. Photovoltaic Effect in Ideal Carbon Nanotube Diodes. *Appl. Phys. Lett.* **2005**, *87*, 073101−1−3.

(29) Blöchl, P. E. Projector Augmented-Wave Method. *Phys. Rev. B* **1994**, *50*, 17953−17979.

(30) Kresse, G.; Furthmüller, J. Efficient Iterative Schemes for *Ab Initio* Total-Energy Calculations Using a Plane-Wave Basis Set. *Phys. Rev. B* **1996**, *54*, 11169−11186.

(31) Perdew, J. P.; Burke, K.; Ernzerhof, M. Generalized Gradient Approximation Made Simple. *Phys. Rev. Lett.* **1996**, *77*, 3865−3868.

(32) Kresse, G.; Joubert, D. From Ultrasoft Pseudopotentials to the Projector Augmented-Wave Method. *Phys. Rev. B* **1999**, *59*, 1758−1775.